Journal of Marine Systems 196 (2019) 1–13

Contents lists available at ScienceDirect

Journal of Marine Systems

journal homepage: www.elsevier.com/locate/jmarsys

Biogenic matter characteristics, deposition flux correction, and internal phosphorus transformation in Jiaozhou Bay, North China

Jin Liu[a,b,d], Jinming Song[a,b,c,d,*], Huamao Yuan[a,b,c,d,*], Xuegang Li[a,b,c,d], Ning Li[a,b,c,d], Liqin Duan[a,b,c,d]

[a] Key Laboratory of Marine Ecology and Environmental Sciences, Institute of Oceanology, Chinese Academy of Sciences, Qingdao 266071, China
[b] Laboratory for Marine Ecology and Environmental Science, Pilot National Laboratory for Marine Science and Technology (Qingdao), Qingdao 266237, China
[c] University of Chinese Academy of Sciences, Beijing 100049, China
[d] Center for Ocean Mega-Science, Chinese Academy of Sciences, Qingdao 266071, China

ARTICLE INFO

Keywords:
Biogenic elements
Sediment resuspension
Phosphorus sink-switching
Organic matter degradation
Jiaozhou Bay

ABSTRACT

Sediment resuspension in coastal environments is associated with both nutrient repartitioning and with the biological carbon pump, which are further linked to climate change, eutrophication, and marine pollution. To explore these relationships, a resuspension framework, including surficial/core sediments and settling trap-collected particles (TCPs), was assessed in the Jiaozhou Bay (JZB) to examine the behavior and fate of particulate biogenic elements (C, N, P and Si). Resuspension-mediated differences in the concentrations of numerous biogenic proxies were significant and mainly corresponded to selective upwelling of fine-sized, nutrient-enriched particles, to autochthonous organic matter degradation below the trap-deployed level comprising water column transportation and long-term retention at the sediment-water interface. This is further reinforced by smaller inorganic carbon concentrations in sediments and origin-indicating stoichiometric ratio records (OC:ON, OC:OP). Nevertheless, biogenic silica (BSi) exhibited a near homologous concentration and had the largest preservation efficiency. Three principal components, representing production and preservation, remineralisation, and a particle-size effect, accounted for 55.5%, 14.0%, and 9.1% of the total variance, respectively. After calibration, the primary sinking flux was two orders of magnitude smaller than the measured absolute sedimenting flux. Also, the limited bottom achieving contribution with a maximum of 28.3% for freshly biogenic particles produced in autumn/winter circumstances with low primary productivity was inferred. The recurrent resuspension processes in JZB demonstrated that 5–12 cycles of similar or higher intensity resuspension was required before freshly-formed biogenic particles could ultimately be integrated into the sediments. Regarding the internal P sink-switching mechanism, the previously transformed Fe-bound fraction across the estuarine salinity gradient has limited application under offshore redox oscillations, whereas near-quantitative transfer of dissolved P from remineralized organic matter to authigenic carbonate fluorapatite could substantially reduce its bio-availability in resuspended particulate P.

1. Introduction

Sediment resuspension in energetic and dynamic continental margins, caused by natural (wind, wave, tide, etc.), anthropological (dredging, trawling, fishing, etc.), and benthos activities (burrowing, biological irrigation, etc.) could invoke myriad interior chemical and physical processes. These processes prominently influence the biogeochemical behaviors of carbon, nutrients, trace metals, and other organic/inorganic pollutants in the water column (Hung et al., 2016; Kalnejais et al., 2010; Lin et al., 2016; Song and Li, 2018), as well as affecting the exchange of these entities at the sediment-water interface (SWI) (Rutgers van der Loeff and Boudreau, 1997; Ye et al., 2013), and thus, further linking these processes to climate change, eutrophication, and marine pollution. For example, entrainment of seabed organic matter and reduced chemical species into the water column can increase remineralisation and oxidation rates, thereby decreasing oxygen concentrations in bottom waters of some coastal environments (Moriarty et al., 2017). Moreover, the flux of sinking particulate organic carbon (OC) can be significantly overestimated compared with primary production (PP) near the surface, with approximately 30 to 93%

* Corresponding authors at: Key Laboratory of Marine Ecology and Environmental Sciences, Institute of Oceanology, Chinese Academy of Sciences, 7# Nanhai Road, Qingdao, Shandong 266071, China.
E-mail addresses: jmsong@qdio.ac.cn (J. Song), yuanhuamao@qdio.ac.cn (H. Yuan).

https://doi.org/10.1016/j.jmarsys.2019.04.001
Received 11 December 2018; Received in revised form 30 March 2019; Accepted 5 April 2019
Available online 11 April 2019
0924-7963/ © 2019 Elsevier B.V. All rights reserved.

assigned to active sediment resuspension in the East China Sea (Hung et al., 2016; Hung et al., 2013). Such overestimation might lead to a considerable imbalance for carbon input and burial model calculations in continental margins (Hung et al., 2016). Therefore, the internal biogeochemical processes caused by resuspension, and their quantitative relationships, must be identified and appropriately constrained.

The production and destruction of autochthonous biogenic particles (living and dead organic matter and mineral skeletons) are dominant agents in transporting biogenic elements (C, N, P and Si) in oceanic water columns, and in regulating the concentration and availability of these elements (Yu et al., 2012b) through such mechanisms as the biological pump, in which nutrient-containing compounds are exported via biological processes from the surface to the deep ocean (Zhang et al., 2006a). The major part of this organic supply is subject to extraordinarily low preservation efficiency within geochemical records (Liu et al., 2016). As such, before being permanently buried, this primary organic material is substantially altered in terms of composition and abundance through the diagenetic reactions taking place in the surface sediments (Rutgers van der Loeff and Boudreau, 1997). Therefore, the highly selective resuspension of finer deposited fractions, along with the closely associated, more aged and refractory organic matter, would influence the organic signature of particles in the water column and, therefore, also influence zooplankton and other heterotrophic organisms that feed on this fraction (Hwang et al., 2017; Mayer, 1994). Additionally, an increased suspended load during resuspension/sedimentation processes increases the available surface area for particle-water interaction, favoring an increase in reaction rates per volume of water and interfacial repartitioning of the nutrients, as well as elevating turbidity and affecting the depth of the euphotic layer, phytoplankton photosynthesis, and the diel migration of zooplankton (Song and Li, 2018; Yurkovskis, 2005). Besides the internal source of particulate nutrients, the release of C, N, P and Si in inorganic dissolved form following biological degradation mechanisms can be enhanced by sediment disturbance. Further upward injection triggered by resuspension (Yu et al., 2013) can facilitate the phytoplankton growth demand and potentially impact the phytoplankton community structure (Song and Li, 2018). Given the fact that numerous coastal environments are suffering severe threats of eutrophication from intensive anthropological activities over the last few decades (Kang et al., 2017), this internal P release following resuspension, possibly with a particle-bound P loading about the same as the tributary contribution (Matisoff and Carson, 2014), would further aggravate and prolong eutrophication, leading to water quality deterioration and hindering efforts to limit nutrient loading through policy-making. Hence, it is important to study the distribution of P speciation in resuspended particles to understand the cycle of P and identify its potential bioavailability.

In order to assess the sinking particle flux and related biological carbon pump with respect to the advection or vertical mixing, and the nature and extent of biogeochemical transformations, numerous studies using time-series sediment trap moorings have been carried out (Honjo et al., 2008; Turner, 2015). Many of these studies have been conducted in open ocean environments, where particle flux is mainly controlled by production and export of biogenic particles from the overlying surface ocean, and have generally focused on the flux attenuation, biogenic matter degradation, and remineralisation during the vertical transit from surface to deep waters, as well as their sedimentation. Much remains to be understood, however, concerning the reverse process (i.e. resuspension-induced transportation from the underlying sediment to the upper water column) in coastal environments where allochthonous biogenic/lithogenic particles are incorporated into both surface autochthonous and bottom sedimentary end-members. Since there is no a priori reason why the concentration change should be attributed solely to reactions occurring during the initial sinking process and in the sediment, but not during resuspension (Rutgers van der Loeff and Boudreau, 1997), a comparative analysis of biogenic elements between sediment and sinking particles would provide crucial information for elucidating the mechanisms related to internal cycling of particles resulting from resuspension. Such analysis would also allow improved evaluation of the processes influencing the uptake, storage, and transformation of carbon and nutrients in the marine environment (Hung et al., 2013). Furthermore, such assessment would have implications for carbon and nutrient export from coastal waters to the open ocean (Painter et al., 2017).

Therefore, in the present study, we examined the behavior and fate of particulate biogenic elements (C, N, P and Si) in different substances, including surficial/core sediments and settling trap-collected particles (TCPs), which comprise resuspended particles and the co-occurring biogenic, authigenic, and lithogenic particles from the upper water of Jiaozhou Bay (JZB), to correctly decipher the biogeochemical signal in this coastal environment. Accordingly, three main questions concerning internal cycling of organic matter were addressed: (1) what are the principal sources of the settling organic matter and the organic matter that becomes incorporated within the bottom sediment? (2) what are the effects of resuspension upon the quantity and character of organic materials sinking through the water column? (3) what quantitative relationships exist between the sinking and sedimented flux of particulate biogenic parameters in JZB? Furthermore, we use this resuspension framework to discuss the internal P transformation mechanism based on the compartment-specific partitioning signatures of various P fractions.

2. Materials and methods

2.1. Study area

The JZB (35°58′–36°18′ N, 120°04′–120°23′ E), a typical semi-enclosed bay situated on the west of the Yellow Sea and the southeast of the Shandong Peninsula (Fig. 1a), is vulnerable to the natural changes and anthropogenic activities relating to the rapid industrialization and urbanization in the surrounding regions over the past three decades. The water area of JZB is approximately 370 km^2 with an average depth of 7 m (Song et al., 2016). About 10 rivers, notably the Daguhe, Moshuihe, Baishahe, Licunhe, and Yanghe Rivers, disgorge seasonally into the bay with variable freshwater discharges and sediment loads, along with metal and organic pollutants that have led to a deterioration in environmental quality of the region (Liang et al., 2018). The mouth of JZB is quite narrow, so the poor water-exchange between the inside and outside of the bay may seriously constrict the diffusion of pollutants and the self-purification of the bay. Even though the construction of a water conservancy project has reduced the river discharge, the agricultural, industrial, and urban domestic wastewater discharged directly from point sources, and indirectly via surface runoff and groundwater, have made the sedimentary biogenic proxies (e.g. bioavailable P) an increasing trend since the 1980s (Kang et al., 2017; Song et al., 2016). Furthermore, the sudden and large amounts of nutrient inputs from atmospheric wet/dry deposition may enhance PP prominently (Xing et al., 2017; Xing et al., 2018). All the above factors have influenced the external transportation and internal cycling of biogenic elements in JZB during the last few decades.

2.2. Sampling

The sampling strategy in the investigated marine areas was a compilation of three sample series (Fig. 1b): (1) Two mooring McLane® Mark 78H Time Series sediment traps were deployed five meters above the sea floor—one in July 2016 at station TS1 at a water depth of 15 m, and the other in December 2016 at station TS2 at a water depth of 10.5 m. The sinking particles were collected at a fixed time interval of 24 h, and eight and seven samples were retrieved from stations TS1 and TS2, respectively. (2) Six surficial sediment (SS) samples, numbered from S3 to S8 and stretching over the entire JZB area, were collected in mid-August 2016 using a Van Veen grab sampler. (3) One sediment

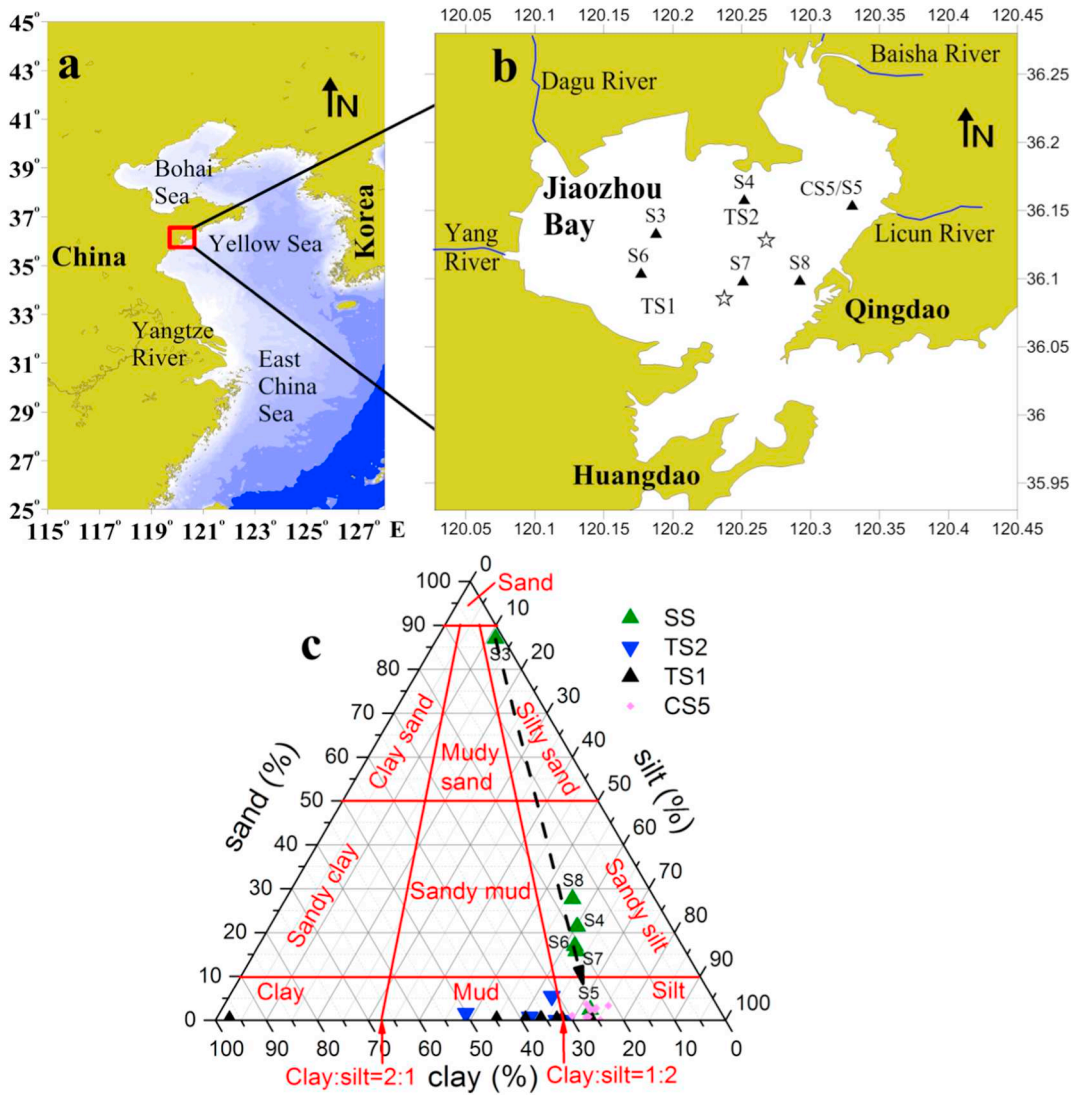

Fig. 1. (a) East China marginal seas and the location of Jiaozhou Bay (inside the red rectangle). (b) Sampling stations in Jiaozhou Bay. Solid black triangles indicate one sediment core and six surface sediment sampling stations, open pentagons denote the trap stations. (c) A ternary map of grainsize classification for trap-collected particles and surface/core sediments. (For interpretation of the references to colour in this figure legend, the reader is referred to the web version of this article.)

core (CS5) with a length of 20 cm was collected at station S5 using a box sampler during the same campaign as the SS sampling. Samples were transported to the laboratory for all analyses. Due to the high particulate concentrations of the bulk sediment-trap samples, the sediment-trap particles were weighed as the difference between the full retrieved bottles and a reference bottle of the same size filled with 0.2-mm filtered seawater. All traps were screened for zooplankton 'swimmers' > 200 μm prior to filtering. Bulk particulate concentrations of biogenic elements (C, N, P and Si) were determined in samples filtered onto pre-combusted HCl-washed glass fiber (GF/F) filters. The sediment core was sectioned at 2-cm intervals and a total of 10 subsamples were obtained. All surface and core sediment subsamples were stored in plastic bags and immediately deep-frozen and lyophilized. Dried aliquots were ground using an agate mortar and pestle for homogenization and prepared for analysis. Data from this study are reported on a dry weight basis.

2.3. Chemical measurements

Total carbon (TC) and OC measurements were made on lyophilized samples ground to 200 mesh. The untreated subsamples were analyzed for TC with a Perkin-Elmer model 2400 elemental analyzer. The concentrations of OC were determined in a similar way after treating another set of subsamples with HCl (4 mol L^{-1}) several times until ebullition ceased in order to remove inorganic carbon prior to analysis. Concentrations of inorganic carbon (IC) were equated to the difference between TC and OC. Organic phosphorus (OP) was calculated as the difference between total P (TP) and inorganic P (IP), where TP and IP were determined based on HCl-extractable P (1 mol L^{-1} HCl, 24 h) of combusted (550 °C, 2 h) and non-combusted sediment, respectively (Aspila et al., 1976). The inorganic nitrogen (IN) was extracted in 25 mL 0.1 mol L^{-1} HCl for 2 h. The residue from the IN extraction was treated with alkaline $K_2S_2O_8$ at 124 °C for 1 h to digest organic nitrogen (ON). Reactive N in the HCl and $K_2S_2O_8$ extracts were then determined photometrically following standard procedure using a continuous flow analyzer (QuAAtro, Bran-Luebbe Inc., Germany). The concentration of IN is the sum of NH_4-N, NO_3-N, and NO_2-N. The detection limits for NH_4-N, NO_3-N, and NO_2-N were 0.25, 0.40 and 0.01 μmol L^{-1}, respectively. National standard references were used to determine the precision and accuracy of the analysis. The precisions and recoveries for all nutrient species were better than 5% and between 95.0 and 105.1%, respectively. Total nitrogen (TN) was taken as the sum of IN and ON.

Determination of biogenic silica (BSi) was performed by the strong alkaline leaching method (Mortlock and Froelich, 1989), together with

determination of the slope for mineral correction (DeMaster, 1981, 1991). The BSi extractions were made on ~100 mg aliquots of sediment samples, mixed well with 40.0 mL of 2 mol L^{-1} Na_2CO_3 solution, after treatment with acid and peroxide to remove carbonate and organics, and placed in a water bath preheated to 85 °C. An aliquot of 125 μL of clear centrifugation supernatant was taken from the extraction solution after 1, 2, 3, 4, 5, 6, 7, and 8 h, then measured by the molybdate blue spectrophotometric method. The concentrations of BSi were then converted to weight permille SiO_2 of dry bulk sediment, together with determination of the slope for mineral correction (DeMaster, 1981, 1991). The analytical precision was less than ± 2% (Liu et al., 2002).

Ground sediment was digested with a mixture of HF-HNO_3-$HClO_4$ at 150 °C for 48 h. Major components (Al_2O_3 and Fe_2O_3) were determined by inductively coupled plasma mass spectrometry (ICP-MS) after dilution in trace-metal grade 2% HNO_3. The accuracy of the total analysis was assured using the standard reference materials GSD-9 and GSS-15. The recoveries of Al_2O_3/Fe_2O_3 were 99.34/101.23% for GSD-9 and 95.15/99.22% for GSS-15, respectively. Reactive Fe_2O_3 was determined as the sum of five Fe fractions using the sequential selective extraction procedure modified from Poulton and Canfield (2005) and converted to weight permille Fe_2O_3 of dry bulk sediment, which included exchangeable Fe and carbonate Fe, poorly-crystalline Fe oxide, crystalline Fe oxides, magnetite, and organic matter-bound fractions.

2.4. Sequential extraction of P

Fractionation of sedimentary P by sequential extraction (SEDEX) is an effective method to investigate the cycling and ecological significance of P in waters (Yu et al., 2012a). The SEDEX method employed in the present study discriminates between the various chemical species of sedimentary P into exchangeable or loosely-sorbed P (P1), iron-bound P (P2), authigenic P (P3; this includes authigenic carbonate fluorapatite, biogenic apatite, and $CaCO_3$-associated P), detrital P (P4) and organic P (OP) (Huerta-Diaz et al., 2005; Ruttenberg, 1992). Briefly, about 0.15 g of homogenized sediment was weighed and loaded into a 50-mL centrifuge tube, and P1 was extracted with 1 mol L^{-1} $MgCl_2$ (pH = 8) for 2 h. In order to avoid sediment matrix effects, the sediment residue was washed twice with 1 mol L^{-1} $MgCl_2$ (pH = 8). The residue was then extracted with citrate-dithionite-bicarbonate (CDB) solution (0.22 mol L^{-1} $C_6H_5Na_3O_7$ + 0.11 mol L^{-1} $NaHCO_3$ + 0.11 mol L^{-1} $Na_2S_2O_4$) (pH = 7.6) for 8 h to obtain P2. Next, the sediment residue was extracted with 1 mol L^{-1} Na-acetate buffer (pH = 4) for 6 h to obtain P3. Finally, the sediment residue was extracted with 1 mol L^{-1} HCl for 16 h to obtain P4. Between each process, from P2 to P4, the sediment residue was washed twice with 1 mol L^{-1} $MgCl_2$ (pH = 8) and once with high purity water. The detailed process has been described previously by of Yang et al. (2016).

The acid extraction solution was neutralized and pre-treated prior to analysis by the phosphomolybdenum blue method. The sum of the above four P forms (P1, P2, P3, and P4) determined by the SEDEX scheme was not significantly different than with independent measurement of IP in the same samples (ANOVA, $p < 0.05$), suggesting that the SEDEX scheme was a valid method for determining inorganic P forms in sediments. OP in the P1 and P3 fractions has been observed to be extremely low (Kang et al., 2017), thus we ignored the presence of OP in these fractions. Since it has been previously demonstrated that the OP concentration can be underestimated when using the SEDEX scheme (Ruttenberg, 1992), we determined the OP concentration by the method described in Section 2.3.

2.5. Grain size analysis

Granulometric analysis was carried out by using a Mastersizer 2000 instrument (Malvern Ltd., UK) after removing calcareous cement and shell materials with 5 mL of HCl solution (3 mol L^{-1}). The measurement range was 0.01–1200 μm, with a resolution of 0.01 Φ and an error of replicate measurements < 3%.

2.6. Statistical analysis

The calculation of the mean values, the standard error of the mean values (E), the minimum/maximum values, and all multiple comparison tests between TCPs, SS, and CS5 were performed with MATLAB R2014a®. Pearson correlation coefficients were calculated using SPSS version 18.0 software. Unless otherwise indicated, a significance level of $\alpha = 0.05$ was applied for all statistical analyses. Principal component analysis (PCA), which has been widely used to explore environmental datasets that are large and spatially diverse (Liu et al., 2018), was also conducted with the SPSS version 18.0 software for the whole dataset including biogenic elements, granulometric parameters, and Al_2O_3/Fe_2O_3 in TCP, SS and CS5. In this study, a varimax rotation was included to maximize the loading of variance onto each principal component to assist in data interpretation (Kaiser, 1958).

3. Results

3.1. Grain size characteristics

A coupled sedimentation and resuspension physical model was developed in a companion paper (Liu et al., in prep), so the grain size distribution of the particles and sediments in the JZB are simply described in the present study. The average medium grain size (D50) was 5.45 ± 0.87 μm for TS1 and 5.91 ± 0.47 μm for TS2, significantly smaller than that of 38.7 ± 21.42 μm for SS, and that of 9.94 ± 0.46 μm for CS5 (Table 1). The mean proportion of sand and clay showed wide variation, with SS having higher sand percent and less clay percent than CS5 and TCPs (Table 1). Silt constituted the largest proportion and this proportion did not significantly differ among different samples, ranging from 54.18 ± 8.82% to 72.7 ± 0.74% (Table 1). Based on the ternary map of sediment category (Fig. 1c), TCPs mainly fell within the mud category, SS within sandy silt, and CS5 within silt (Folk and Ward, 1957). Combined with the spatial dispersal of SS in the JZB (Fig. 1b, c), a straight line drawn from station S3, via S8, S4, S6 and S7, to S5 generally suggested that with longer offshore distances, and shorter distances to the trap installation points, the more similar were the granulometric compositions of SS and TCPs, with the exception of S5, which has a suddenly reduced hydrodynamic force (Song et al., 2016). The sedimentary records of D50 and clay percentage are illustrated in Fig. 2a and b, which reveal large fluctuations with an overall decreasing down-core trend for D50 and an increasing down-core trend for clay percentage over the 20 cm depth profile.

3.2. Geochemical structure of biogenic elements in TCPs and sediments

The characteristics of biogenic elements for settling particles and surface/core sediments are summarized in Table 1. Comparing the two sediment trap stations, there was no significant difference in the biogenic parameters, except that the TC and IC contents at TS1 station were significantly higher than those at TS2 station. Although the concentrations of IN, IP, and BSi in the TCPs and sediments showed no significant differences, the concentrations of most biogenic parameters in TS1 and TS2 were significantly higher than their analogues in surface/core sediments, including TC, IC, OC, TN, ON, TP and OP. Among them, the TC concentration of TCP was roughly 1.69–1.98 times SS and 1.12–1.31 times CS5; the IC concentration of TCP was about 2.48–3.49 times SS and 1.72–2.43 times CS5; the OC concentration of TCP was about 1.45–1.51 times SS and similar to that of CS5; the TN concentration of TCP was about 1.91–2.70 times SS; the ON concentration of TCP was about 1.90–2.51 times SS; the TP concentration of TCP was about 1.12–1.22 times SS, similar to that of CS5; the OP concentration of TCP was about 1.75–2.10 times SS and 1.24–1.50 times CS5 (Table 1). The concentrations of IN in SS and the TCPs were quite lower than ON and TN, ranging from 12.3 mg g^{-1} to 29.11 mg g^{-1}. The changes of IP concentrations between the different samples were trivial,

Table 1
Characteristics of physical and chemical parameters for trapped particles and surface/core sediments (± standard deviation of the mean), letters represent significant differences ($p < 0.05$).

Parameters	TS1 (n = 8)	TS2 (n = 7)	SS (n = 6)	CS5 (n = 10)
TC (mg g^{-1})	10.94 ± 0.28 a	9.34 ± 0.13 b	5.51 ± 0.74 c	8.3 ± 0.13 b
IC (mg g^{-1})	4.61 ± 0.17 a	3.27 ± 0.19 b	1.32 ± 0.22 c	1.9 ± 0.15 c
OC (mg g^{-1})	6.32 ± 0.14 a	6.07 ± 0.11 a	4.19 ± 0.66 b	6.4 ± 0.11 a
OC:TC (%)	57.86 ± 0.67 a	65.07 ± 1.63 ab	74.17 ± 5.35 b	77.24 ± 1.49 b
TN (μg g^{-1})	1154 ± 124.48 a	887.26 ± 30.5 a	464.43 ± 87.39 b	–
IN (μg g^{-1})	20.8 ± 4.56 a	29.11 ± 6.46 a	12.3 ± 1.35 a	–
ON (μg g^{-1})	1133.2 ± 124.22 a	858.15 ± 27.79 a	452.13 ± 87.56 b	–
ON:TN (%)	98.14 ± 0.37 a	96.77 ± 0.7 a	96.11 ± 1.76 a	–
D50 (μm)	5.45 ± 0.87 a	5.91 ± 0.56 a	38.7 ± 21.42 a	9.94 ± 0.46 a
Clay (%)	43.13 ± 7.97 a	36.72 ± 3.57 ab	17.32 ± 3.38 b	25.32 ± 0.87 b
Silt (%)	56.87 ± 7.97 a	61.73 ± 3.61 a	54.18 ± 8.82 a	72.7 ± 0.74 a
Sand (%)	0 ± 0 a	1.55 ± 1.01 ab	28.5 ± 12.17 b	1.99 ± 0.51 a
TP (μg g^{-1})	835.18 ± 18.24 a	770.66 ± 11.46 ab	687.52 ± 59.11 b	793.55 ± 11.81 ab
IP (μg g^{-1})	545.99 ± 12.93 a	530.37 ± 10.13 a	550.22 ± 39.37 a	599.13 ± 15.72 ab
OP (μg g^{-1})	289.19 ± 13.28 a	240.29 ± 6.94 ab	137.3 ± 24.59 c	194.42 ± 6.07 b
OP:TP (%)	34.57 ± 1.18 a	31.18 ± 0.81 a	19.1 ± 2.98 b	24.6 ± 1.03 b
BSi (mg g^{-1})	11.7 ± 1.08 a	10.54 ± 0.74 a	9.19 ± 1.99 a	9.58 ± 1.24 a
BSi:OC (mol mol^{-1})	0.37 ± 0.03 a	0.35 ± 0.02 a	0.46 ± 0.09 a	0.3 ± 0.04 a
BSi:ON (mol mol^{-1})	2.48 ± 0.21 a	2.89 ± 0.25 a	5.06 ± 0.83 b	–
BSi:OP (mol mol^{-1})	20.83 ± 1.41 a	22.66 ± 1.37 ab	42.47 ± 10.48 b	25.89 ± 3.76 ab
OC:OP (mol mol^{-1})	56.99 ± 1.75 a	65.49 ± 1.69 ab	90.84 ± 15 b	85.67 ± 2.58 b
OC:ON (mg mg $^{-1}$)	6.86 ± 0.47 a	8.3 ± 0.27 ab	10.42 ± 1.04 b	–
OP:ON (mg mg $^{-1}$)	0.12 ± 0.01 a	0.13 ± 0.01 a	0.12 ± 0.01 a	–
Al_2O_3 (mg g^{-1})	147.8 ± 3.6 a	141.9 ± 3.7 a	131.4 ± 4.7 a	144.6 ± 6.6 a
Fe_2O_3 (mg g^{-1})	60.3 ± 1.9 a	58.4 ± 1.5 a	39 ± 4.2 b	54.7 ± 2.6 a
Reactive Fe_2O_3 (mg g^{-1})	12.16 ± 0.26 a	11.58 ± 0.17 a	8.21 ± 0.99 b	11.64 ± 0.14 a

with a range of 530.37 g^{-1} to 599.55 g^{-1}. Similarly, the concentration of BSi fluctuated around 10 mg g^{-1} with a relatively small degree of variation.

Additionally, to relate the associations between TCPs and CS5 in Table 1, the location of the shaded areas and curves in Fig. 2 give a clear demonstration. The concentrations of OC in CS5 peaked at 9 cm, corresponding to a local D50 minima and clay maxima, where IC concentrations hit the lowest point (Fig. 2c). Resembling their analogues in the TCPs, the concentrations of BSi and molar ratios of BSi:OC oscillated around constant values of 10 mg g^{-1} and 0.35 mol mol^{-1}, respectively, though both exhibited significant drops and ascents at 15 cm and 9 cm, respectively (Fig. 2d and e). While variation with a slight amplitude could be observed in the deeper part of CS5, a monotonic down-core trend of decreasing reactive Fe_2O_3 concentrations for the upper CS5 (< 7 cm) is opposite in pattern to the BSi:OC molar ratios (Fig. 2f).

Compared with the percentages of organic forms of different elements (Table 1), the OC:TC ratio of TCP was 57.86%–65.07%, which was lower than that of 74.17%–77.24% in the sediments. However, the OP:TP ratio of TCP (31.18%–34.57%) was higher than the corresponding parameters of the sediments (19.1%–24.6%), and the ON:TN ratio of particulate matter was 96.77%–98.14%, parallel with its

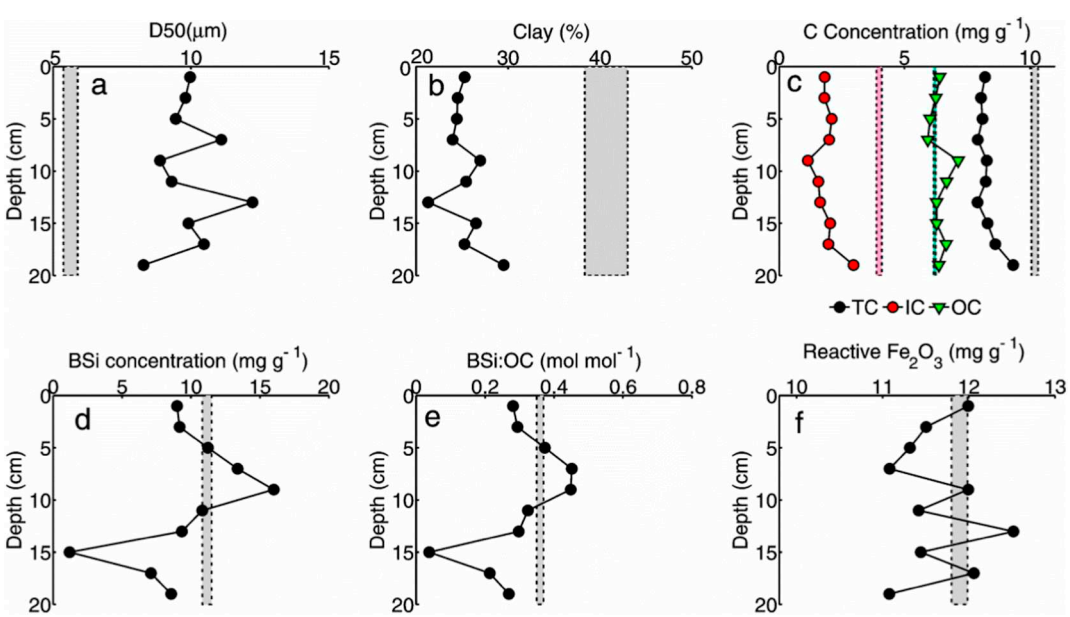

Fig. 2. Sediment proxy records from core sediment CS5. (a) D50; (b) clay content; (c) concentration of TC, IC and OC; (d) BSi concentration; (e) molar ratio of BSi:OC and bio-available Fe_2O_3 concentration; (f) molar ratio of OC:bio-available Fe_2O_3 and OP:bio-available Fe_2O_3 (Shadows indicate the mean value ± standard error of their TCP analogues).

analogue in SS (96.11%). This means that C and N predominantly existed in organic form while P was mainly present in inorganic form. In terms of the stoichiometric ratio of biogenic elements, the proxies typically showed larger quantities for surface/core sediments than for the TCPs (Table 1), with the exception of OP:ON, which displayed a parallel trend between TS1 and the sediments (SS and CS5), but exhibited slightly higher values for TS2. The BSi:OC, BSi:ON, BSi:OP, and OC:OP of SS were roughly 1.24–1.31 times, 2.04–3.79 times, 1.87–2.04 times, and 1.38–1.60 times greater, respectively, than their analogues in TCP. Likewise, the BSi:OP and OC:OP of CS5 were approximately 1.14–1.87 fold and 1.38–1.60 fold larger than those in TCP. Similar to clay content, the concentrations of Al_2O_3/Fe_2O_3 and reactive Fe_2O_3 exhibited an increasing trend, with a sequence of SS < CS5 < TCP.

Comparing the correlation coefficients between biogenic elements, grain size parameters (D50, Clay and Sand), and terrigenous 'reference' oxides (Al_2O_3/Fe_2O_3) (Supporting information A, Table A1), OC, TC, ON, TN, OP and TP in SS were significantly correlated with grain size parameters and with Al_2O_3/Fe_2O_3. TC:IC ratios in CS5 were also significantly correlated with grain size parameters and with Al_2O_3/Fe_2O_3 ($r = -0.635$, $p = 0.049$ for TC versus D50; $r = 0.837$, $p = 0.003$ for TC versus clay; $r = 0.650$, $p = 0.042$ for IC versus Fe_2O_3; $r = 0.669$, $p = 0.034$ for IC versus Al_2O_3). In the SS dataset, the ranges of the absolute value of correlation coefficients between TP, OP, OC, and ON versus the three particle size parameters and Al_2O_3/Fe_2O_3 were 0.845–0.906, 0.956–0.982, 0.873–0.974, 0.921–0.990, respectively. On the contrary, all biogenic parameters exhibited no statistically significant relationship with grain size parameters and terrigenous 'reference' oxides, with the exception of TS1-OP and TS2-TP/IP. At station TS1, the correlation coefficients between OP and the three particle size parameters (D50, clay, and sand) were −0.804, 0.747 and −0.747, respectively. At station TS2, the correlation coefficients between TP and the particle sizes (clay and sand) were −0.882 and 0.961, and IP versus clay and sand were 0.961 and 0.990, respectively.

3.3. Distribution of various P species

The concentrations of various P species in TCPs and sediments are shown in Figs. 3 and 4. The average relative contribution of the five defined P fractions to TP was OP (34.57%) > P4 (25.64%) > P3 (22.96%) > P2 (15.42%) > P1 (1.41%) for TS1, OP (31.18%) > P4 (26.93%) > P3 (26.21%) > P2 (13.89%) > P1 (1.78%) for TS2, P3 (39.27%) > P4 (26.27%) > OP (19.10%) > P2 (13.07%) > P1 (2.29%) for SS, and P3 (31.36%) > P4 (27.64%) > OP (24.60%) > P2 (13.32%) > P1 (3.08%) for CS5. OP was the largest component of the TCP-TP pool (208.55 μg g^{-1}–346.14 μg g^{-1}) while the quota of P3 (182.21 μg g^{-1}–408.69 μg g^{-1}) was highest for the SS/CS5-TP pool (Figs. 3 and 4). Both fractions had larger fluctuations than the others. Additionally, it is noteworthy that the concentrations of OP were strongly and negatively correlated with the concentrations of P3 ($r = -0.56$, $p = 0.00$) for the entire dataset, and the two mirrored of one another in terms of concentration and percentage along the depth profile (Fig. 4). There was a significant positive correlation ($r = 0.65$, $p = 0.00$) between OP and P2 overall, while the variation of P2 with depth was dampened due to its low concentration and small percentage (Fig. 4). Among the four forms of IP, P4 was dominant and exhibited a relatively narrow concentration range (177.68 μg g^{-1}–255.92 μg g^{-1}) for TCP and a wide range (95.05 μg g^{-1}–240.97 μg g^{-1}) for sediments; however, P4 contributions were relatively constant for both TCP and SS/CS5 samples. The P1 component contributed a consistently small proportion to the total P pool in all samples.

The correlation coefficients of the various P fractions versus the biogenic elements, the granulometric parameters, and Al_2O_3/Fe_2O_3 are tabulated in Supporting information A, Table A2. Strong and significant relationships of P1 only occurred with silt ($r = 0.600$, $p = 0.000$) and sand ($r = -0.599$, $p = 0.000$), whereas P2, P4, OP, and TP additionally exhibited significant positive correlations with the concentrations of the biogenic elements (TC, IC, OC and ON) and significant negative correlations with the stoichiometric ratios of the biogenic elements (BSi:ON, BSi:OP, OC:OP and OC:ON). Still, it is worth mentioning that P3 exhibited significant negative correlations with the concentrations of the biogenic elements (TC, IC, OC and ON) but no correlation with most of the stoichiometric ratios, excluding OC:OP.

4. Discussion

Horizontal transported and/or locally resuspended particulate matter appears to be a major source of particles in the coastal environment, unlike open ocean sites in which particle fluxes are mainly controlled by pelagic processes. In this study, the concentration, geochemical characteristics, and sedimentation flux of different biogenic components (C, N, P and Si) in sinking particles and sediments were studied in an attempt to interpret the mixing mechanism of two different sources—namely, primary production in the overlying water and resuspended particulate matter from the bottom. Another potentially important source of particulate matter in the continental shelf margin environment, terrestrial material is contained in the above two sources according to the changes of local material migration patterns.

4.1. Sources and characteristics of biogenic elements

Two factors may help explain the substantially higher concentrations of biogenic parameters (TC, IC, OC, TN, ON, TP and OP) for the TCPs (Table 1). First, resuspended particles collected by sediment traps contained a greater proportion of fine-grain-sized, more easily resuspended particulate matter than did the SS, which is evidenced by the significantly smaller D50 granulometric composition of the TCPs (Table 1, Fig. 1c). Fine particles, such as clay and colloidal materials, are generally surface-active and contain Fe/Mn oxide surface coatings (Liu et al., 2018) thus, resuspended material would be enriched in organic constituents relative to non-suspended, coarse fractions. Such size-dependent effects could occur in organic components of SS, showing higher concentrations in tranquil/quiescent stations (S5) than other near-shore but more hydrodynamic stations (S3, S4, S6 and S8) (Song et al., 2016). Temporary resuspension of organic-carbon-rich, fine-sized sediment particles may also help explain the observation that the surficial sediments typically had smaller clay percentages and lower OC and BSi concentrations than did sediments a few centimeters deeper (9 cm in Fig. 2). The deeper burial may be adequate to prevent selective winnowing of small particles by water turbulence. The second factor involves destruction of organic matter during water transportation processes and long-term retention at the SWI. Microscopic examination of sinking particles in the Yangze River estuary revealed the presence of both inorganic mineral particles and biogenic aggregates, containing larvacean houses, fecal pellets, diatoms, and miscellaneous aggregates, as is generally consistent with that collected in the deep sea (Zhang et al., 2006c). Therefore, the ubiquitous and abundant macroscopic organic aggregates in the coastal environment would result in no observable relationship between biogenic proxies and particle size parameters or terrigenous 'reference' oxides in the TCPs (Table A1). In most cases, the presence of more nutrient-enriched aggregates increases the nutritional content of TCPs (Meinhard et al., 2002). On the other hand, fine-grained minerals have been associated more closely with organic matter based on the significantly stronger correlation between these indicators in SS (Table A1) (Mayer, 1994), where this organic matter is presumably aged and more refractory in nature after being subjected to substantial remineralization processes (Pusceddu et al., 2005).

The second factor is also supported by the stoichiometric ratio of biogenic elements used to indicate the origin of organic matter. The mean values of the OC:ON mass ratios were 6.86 ± 0.47 for station ST1 and 8.3 ± 0.27 for station ST2, which are consistent with a phytoplankton source (Holligan et al., 1984) and indicate that the principal source of OC in the TCPs was in situ algae, cyanobacteria, and aquatic

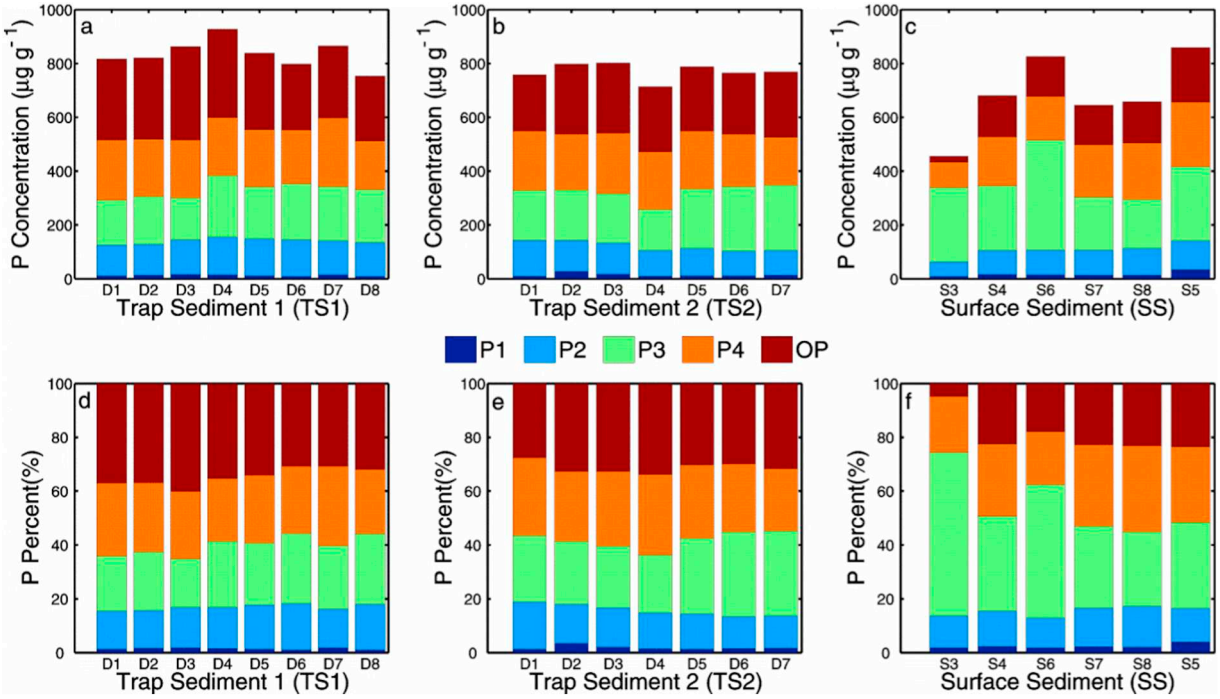

Fig. 3. The average concentrations and percentages of P in the five defined fractions (P1, exchangeable or loosely-sorbed P; P2, iron-bound P; P3, authigenic P; P4, detrital P and OP, organic P).

plants (Table 1). The relatively higher mass ratio of OC:ON in SS (10.42 ± 1.04) would suggest preferential regeneration of N relative to C particularly during the early decomposition stages (Liu et al., 2016). Such corresponding increasement from sinking/resuspended and sedimentary OC:ON ratio has been observed for several sub-tidal and shallow-sea environments (Lamb et al., 2006). However, it was noteworthy that an additional greater contribution from allochthonous matter derived from higher plants to the source of the OC in SS could also partly explain such increase, therefore reflecting a mixing effect (Hedges and Mann, 1979; Liu et al., 2016). This may be attributable to the refractory nature of exogenous OC since labile endogenous organic matter that is stoichiometrically similar to marine plankton is

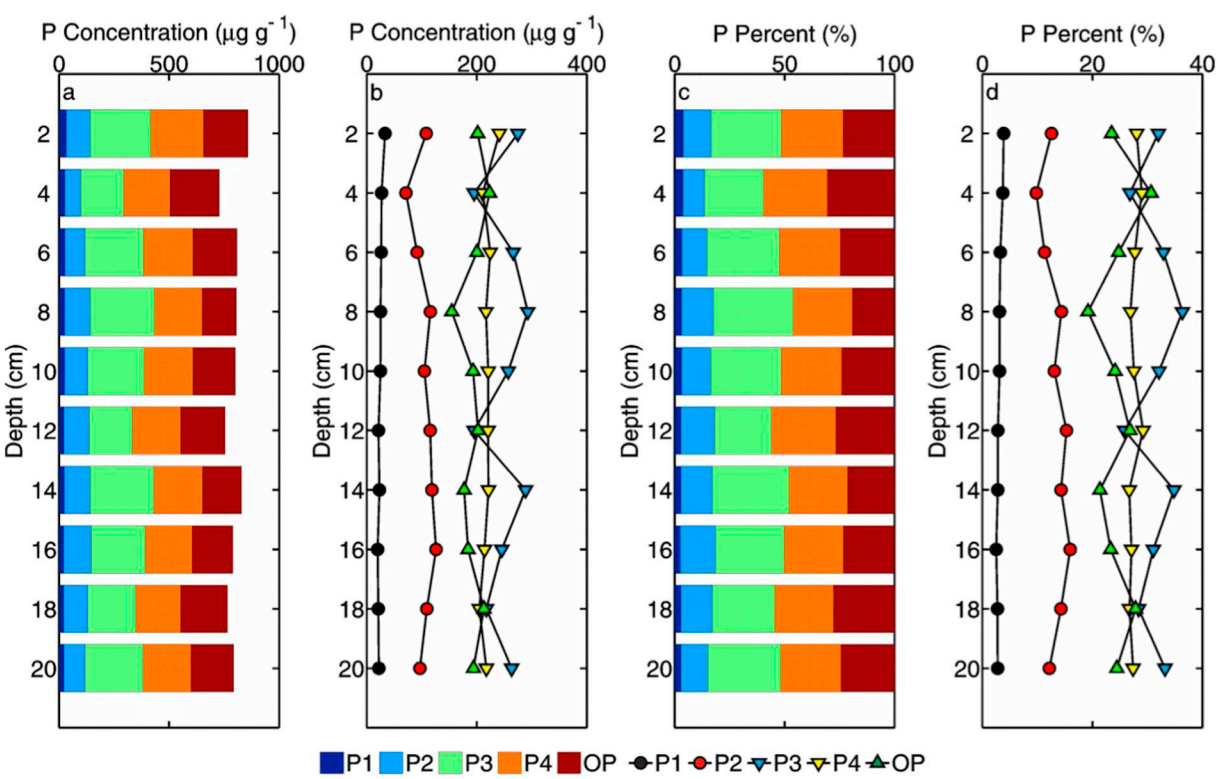

Fig. 4. The CS5 depth profile of concentrations and percentages of the five defined P fractions (P1, exchangeable or loosely-sorbed P; P2, iron-bound P; P3, authigenic P; P4, detrital P and OP, organic P).

preferentially remineralized upon the same deposition path of the sedimentary particulates (Prahl et al., 1980). Therefore, the residual organic matter remaining and buried in the bottom sediments would integrate more terrestrial organic matter, leaving the greater allochthonous signatures imprinted in SS (Meyers et al., 1984). A two end-member $\delta^{13}C$ mixing model previously employed to differentiate terrestrial versus marine sources has demonstrated that, 20–55% of total OC in JZB sediments was terrigenous, which was derived from a mixture of woody and non-woody angiosperms and moderately degraded (Kang et al., 2017; Yang et al., 2011). Based on available carbon isotope data from our sinking particle samples, the $\delta^{13}C$ values were averaged at −22.03‰ (Liu, unpublished data), which was similar with net-towed phytoplankton (mean = −22.07‰) in JZB (Xu and Yang, 2007), but also within the range of C3 plants and marine plankton (Ni et al., 2015), and a mean 43% terrigenous OC in settling particles was solved using the same binary $\delta^{13}C$ mixing model. In this circumstance, it is difficult to distinguish between the effects of decomposition and changes in carbon source, and to compare marine quotient in particles versus sediments, when interpreting bulk OC:ON and $\delta^{13}C$ records.Fortunately, the molar ratio of OC:OP has been widely used to explain the deposition mechanism, source, and degradation characteristics of P, also unravel the above dilemma. The OC:OP ratios of SS and CS5 were 90.84 ± 15 and 85.67 ± 2.58, respectively, which were significantly higher than in the corresponding TCPs (56.99 ± 1.75 and 65.49 ± 1.69, respectively; Table 1), same variation tendency with OC:ON. Given the OC:OP ratio of terrestrial plants in the range of 800–2050 on a molar basis (Likens et al., 1981), the appreciable discrepancy between land provenance and JZB particle/sediment samples can exclude the possibility of a significant contribution of organic matter derived from terrestrial plants. Thus, a dominant allocate of marine plankon for JZB organic matter and the preferential regeneration of P relative to C could be inferred, i.e. the breakdown of P-rich compounds prior to deposition, owing to multiple cycles of resuspension, low deposition rates, long retention times, and consequently early diagenesis (Ingall and Cappellen, 1990). During degradation of organic matter, regenerated P is generally diffused to the sea-water or interstitial water, or is redistributed to different sedimentary P phases, whose fate was discussed below. Additionally, the undeniable disparity between OC:OP ratios of JZB particles/sediments and that of newly-formed marine plankton, which is 106 on a molar basis (Redfield et al., 1963), may be partially attributable to benthic microorganisms that can utilize and transfer the detrital organic matter into low OC:OP biomass. Bacterial biomass can have OC:OP ratios as low as 50 (Reimers et al., 1989). The suggestion being that the low-density bacterial biomass produced in situ in sediment is more likely to migrate upward within the particulate matter and might also contribute to lower OC:OP values of the TCPs.

The significantly lower concentration of IC in SS/CS5 relative to the TCPs (Table 1) is probably traceable in part to the calcareous shell corrosion at the sea floor, leading to more exposure of unprotected marine OC to microbial decomposition and zooplanktonic feeding (Rutgers van der Loeff and Boudreau, 1997). Metabolic CO_2 produced by aerobic mineralization reduces the CO_3^{2-} concentration in the pore-water of SS, causing dissolution at water depths where calcite is supersaturated (Emerson and Bender, 1981). Additionally, there are various forms of IC in sediments, ranging in size from very fine-grained detrital fragments to whole shells of foraminifera, coccolithophores, along with other calcifying organisms. Most marine $CaCO_3$ has been reported to exist as particles smaller than 63 μm (Gardner et al., 1985) and, therefore, the more easily re-suspended fine $CaCO_3$ particles is also one of the reasons for the high concentration of particulate IC in the TCPs.

The concentrations of BSi in this study (Table 1, Fig. 2d) are consistent with the BSi concentration of ~10 mg g^{-1} in the SS of the Bohai Sea and the Yellow Sea (Li et al., 2010; Ye et al., 2002), but are at the lower limit of BSi concentrations in lakes around the world (below detection to 61.5%) (Frings et al., 2014). The BSi concentrations that we observed are also lower than areas of high biogenic silica fluxes in ocean surface sediments, where BSi concentrations can be as high as 4–45% BSi as found in the Southern Ocean, the North and Equatorial Pacific, and a few upwelling continental margins with abundant nutrients and high PP (e.g. the Gulf of California) (Galloway et al., 2013; Pichevin et al., 2014). The JZB, a coastal environment characterized by seawater mixing with freshwater from rivers, high nutrient fluxes, and high PP, is considered to be a potential area for BSi precipitation and burial. However, similar to other studies (DeMaster, 2002), our data do not provide evidence in support of this scenario. Three possible mechanisms may explain this contradiction. One is the potential dilution of BSi concentrations by deposition of terrigenous detrital materials derived from river channel erosion. Another is the existence of terrigenous sediments in seawater (Loucaides et al., 2010). Such an environment can invoke BSi reverse weathering and enhance lateral transport. Previous research has shown that the rapid transformation of authigenic clay minerals from biogenous opal during early diagenesis of delta sediments leads to a decrease of BSi concentrations (Loucaides et al., 2010; Michalopoulos and Aller, 1995). The third possible mechanism is decomposition of BSi during early diagenesis. If this were the case, a monotonic down-core trend of decreasing BSi concentrations for CS5 might be expected. However, BSi concentrations in the core oscillated around a constant value with substantial declines and inclines. The similarity of the BSi trends between TCP and SS/CS5 provides more support for the suggestion that the losses of BSi by early diagenesis were unlikely to have been the dominant processes.

Regarding the molar BSi:OC ratio of 0.3–0.46 in TCP and SS/CS5, a similar (0.23–0.47) and higher (0.5–0.6) range was discovered in the shallow- (< 30 cm) and deep-sections (> 30 cm, before 1984), respectively, of a sediment core located in the central part of JZB (Liu et al., 2010). This is likely a result of a change in dominant species from large- to small-sized diatoms caused by the decrease in dissolved Si $(OH)_4$/IN ratio in the nutrient input (Liu et al., 2005). However, the shift may also be related to shifts from heavily-silicified to lightly-silicified diatoms or to non-siliceous forms such as dinoflagellates (Liu et al., 2010). This transformation linked with the initial Si:N and Si:C ratios of sinking diatoms may be influenced by the bio-availability of Fe because the molar Si:N uptake ratio for healthy diatoms in normal circumstances is ~ 1 on average and reaches a value of ~ 3 in Fe-stressed diatoms (Brzezinski, 1985). Thus, a reprieve of iron limitation when bioavailable Fe is plentiful reduces $Si(OH)_4$ uptake of diatoms, which could explain the opposing trends between reactive Fe_2O_3 concentrations and molar BSi:OC ratios in the upper part (< 7 cm) of CS5 (Fig. 2e and f). In coastal environments where Fe is supplied mainly by terrigenous input, and should, therefore, not be limiting, the Fe availability may still have modulated silicic acid uptake (Liu et al., 2016).

In comparing the BSi concentration in different constituents (Table 1), the preservation efficiency could be an important issue. The fact that the molar ratios of BSi:OC, BSi:ON, and BSi:OP in all samples were greater than their corresponding Redfield values (0.13, 0.94 and 15) indicates preferential preservation of BSi relative to organic matter, including the OC, ON, and OP proxies (Table 1). Equally, the comparison between OC:OP, OC:ON, OP:ON, and the Redfield molar ratio of C:N:P (106:16:1) may imply a generalized gradient of remineralisation time scales of Si > C > N ≥ P. This inference is supported by dissolved nutrient profiles and measurements of sinking particle fluxes in sediment traps (Boyd and Trull, 2007; Brea et al., 2004). It is noteworthy that the mineralization rate of P is the highest among the biogenic elements in the study area, suggesting that the relevant stoichiometric ratio can effectively indicate the degradation process of organic matter.

In order to better interpret bio-elemental signatures in the JZB, multivariate statistical analyses (PCA) were employed to aid in the identification of the associations between total sediment/particle elemental concentrations and environmental dynamics (Fig. 5). The first

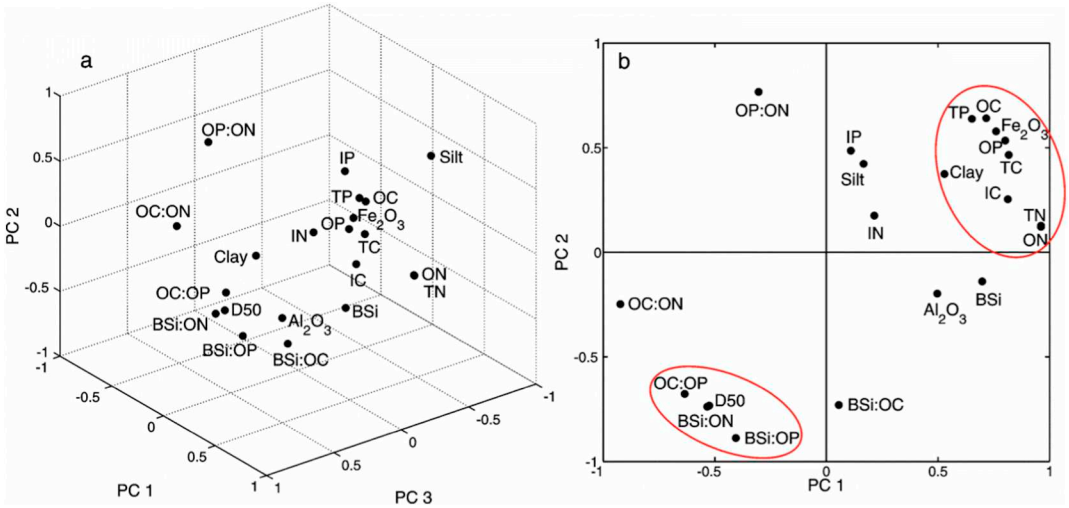

Fig. 5. Principal component analysis of the whole dataset including biogenic elements, granulometric parameters, and Al_2O_3/Fe_2O_3 in TCPs and SS/CS5.

three principal components (PCs) with eigenvalues > 1 from the PCA accounted for 78.6% of the total variance in the whole dataset. PC1 (55.5%) was correlated (loading > 0.70) with Fe_2O_3 and most of the biogenic proxies, including OP, TP, BSi, TC, IC, OC, TN, and ON, suggesting that PC1 represents production and preservation processes of organic matter. Among them, the moderately positive loading of clay (0.53) indicates that fine particles are more conducive to the preservation of organic matter. The variables of high negative loading in PC2 (< −0.70) were generally stoichiometric ratios, i.e. BSi:OC, BSi:ON, BSi:OP, and OC:OP, whereas the high positive loading variable was OP:ON. Among them, the BSi:OP ratio, which reflects the greatest difference in preservation efficiency, had the highest negative loading (−0.89). PC2 (14.0%), therefore, represents the effects of organic matter degradation processes. For PC3 (9.1%), the maximum loading variable was clay (0.717) and the minimum loading was sand (−0.86), representative of the grain-size effect.

4.2. Resuspension estimation and implications for flux attenuation

The end-member mixing model includes surface biogenic particles, characterized by greater OC concentration, and sediments, consisting of low OC concentration. This model has been used to evaluate the resuspension of bottom sediments (Hung et al., 2016). The conceptual model description and calculation for each station is shown in Supporting information B, and the resuspension ratios were 97.8% and 98.01% for stations TS1 and TS2, respectively. Based on quantitative estimation for the fraction of particles resuspended from the bottom, the sinking/sedimenting flux of biogenic proxies was corrected for sediment resuspension per Eq. (1):

$$\text{Corrected Flux} = \text{uncorrected Flux} \times (1-\text{resuspended ratio}) \quad (1)$$

The results show that the uncorrected sinking flux of biogenic proxies at station TS1 were 82.66–247.17 times their sedimented fluxes in underlying sediment, whereas the corrected flux of the biogenic proxies were 1.52–5.44 times the sedimented flux—a difference of two orders of magnitude. Likewise, the uncorrected and corrected settling fluxes of biogenic proxies at station TS2 were 11.79–29.67 times and 0.23–0.59 times their sedimentary analogues, respectively (Table 2). The integrated sedimented fluxes fall somewhere in the middle of the two trap stations, which were deployed at distinct times and within a relatively instantaneous timeframe. Comparing the different organic indexes, the sedimenting flux sequence, from large to small, was OM-Flux (organic matter sinking flux = 2.2 × OC-Flux) > BSi-Flux > OC-Flux > ON-Flux > OP-Flux. Whereas, the sedimented flux exhibited no distinguishable differences between OM-Flux and BSi-Flux, providing further indication that BSi had the highest preservation efficiency. Because the concentration of the biogenic index in SS was typically smaller than that in TCP, overall contributions of resuspended sediment to the sinking particulate load must be much higher than these estimates (Hwang et al., 2017). Therefore, the correction of sedimenting flux in this study often reduces it by two orders of magnitude or more.

Comparing the uncorrected and calculated corrected sinking flux in JZB with analogues in adjacent sea-areas can assess the rationality and accuracy of our flux revision (Table 3). Taking OC-flux as a prime example, the East China Sea was affected by strong resuspension in September 2002, the averaged total (i.e. uncorrected) OC-flux for each water layer was as high as 10.2–160.64 mg cm^{-2} y^{-1}, and the net (i.e. corrected) OC-flux was 35.08 and 4.49 mg cm^{-2} y^{-1} for the nearshore upwelling zone (water depth 55 m) and continental shelf (water depth 88 m), respectively (Zhang et al., 2006b). Correspondingly, contemporaneous uncorrected OC-flux in three sampling stations of the Yellow Sea ranged from 81 to 383 mg cm^{-2} y^{-1}, but the corrected OC-flux decreased to 7.008 mg cm^{-2} y^{-1} (Zhang et al., 2005). Undoubtly, the corrected OC-flux in summer for the same Yellow Sea areas exhibited slightly higher level, 10.59 ± 1.46 mg cm^{-2} y^{-1} (Zhang et al., 2004). Influenced by the artificial aquaculture activities, the corrected annual OC-flux for Sanggou bay, which located in the east coast of Shandong Peninsula, presented greater values (21.2 to 25.9 mg cm^{-2} y^{-1}) than our study and above-mentioned researches (Yang et al., 2014). Therefore, even though the uncorrected fluxes of various parameters are quite different, often spanning two or three orders of magnitude with examples of mass-flux (0.65–97.36 g cm^{-2} y^{-1}), OC-flux (10.22–1390 mg cm^{-2} y^{-1}) and ON-flux (1.06–108.6 mg cm^{-2} y^{-1}) (Table 3), the net fluxes after resuspension correction declined significantly and the differences between JZB and neighboring regions were limited. Among them, the JZB, middle continental shelf of the East China Sea and the Yellow Sea were in the same order of magnitude both for net settling fluxes of OC, ON and TN, while their analogues in nearshore upwelling and aquaculture area were substantially higher due to their high productivity level (Table 3).

The re-release of OC from sedimentary particulate matter into water through mineralization is one of the important factors regulating the air-sea balance of carbon dioxide (Marsay et al., 2015). Numerous studies on the decay profiles of OC sedimentation fluxes have shown that the variation trend can be generalized to the following power equation (Buesseler and Boyd, 2009; Marsay et al., 2015): $F_z = F_{z_0} (z/z_0)^{-b}$ (Eq. (2)), where F_z is the OC-flux at depth z (e.g. sea bottom in this study), normalized to OC-flux at some reference depth, z_0 (e.g. sediment trap in this study), and *b* is the coefficient of flux attenuation. The sedimenting OC-flux (equivalent to F_{z_0}) before and after

Table 2
Sedimenting fluxes of biogenic elements in trap-collected particles and sedimented flux in surface sediments.

Parameters	TS1 (n = 8)	TS1:SS	Corr-TS1	Corr-TS1:SS	TS2 (n = 7)	TS2:SS	Corr-TS2	Corr-TS2:SS	SS (n = 6)
Mass-Flux (g cm^{-2} y^{-1})	49.49 ± 5.09	69.7	1.09 ± 0.16	1.53	8.68 ± 1.41	12.23	0.17 ± 0.03	0.24	0.71 ± 0.20
OC-Flux (mg cm^{-2} y^{-1})	316.23 ± 35.06	106.47	6.96 ± 1.12	2.34	53.41 ± 8.77	17.98	1.06 ± 0.17	0.36	2.97 ± 0.43
TC-Flux (mg cm^{-2} y^{-1})	548.57 ± 63.33	140.30	12.07 ± 2.03	3.09	81.3 ± 12.73	20.79	1.62 ± 0.25	0.41	3.91 ± 0.48
IC-Flux (mg cm^{-2} y^{-1})	232.34 ± 28.5	247.17	5.11 ± 0.91	5.44	27.89 ± 4.09	29.67	0.56 ± 0.08	0.59	0.94 ± 0.14
OP-Flux (mg cm^{-2} y^{-1})	14.31 ± 1.82	130.1	0.31 ± 0.06	2.86	2.09 ± 0.32	19	0.04 ± 0.01	0.38	0.11 ± 0.02
TP-Flux (mg cm^{-2} y^{-1})	41.33 ± 4.06	82.66	0.91 ± 0.13	1.82	6.69 ± 1.04	13.38	0.13 ± 0.02	0.27	0.5 ± 0.04
IP-Flux (mg cm^{-2} y^{-1})	27.02 ± 2.28	69.28	0.59 ± 0.07	1.52	4.6 ± 0.73	11.79	0.09 ± 0.01	0.23	0.39 ± 0.03
ON-Flux (mg cm^{-2} y^{-1})	56.08 ± 7.86	175.25	1.23 ± 0.25	3.86	7.45 ± 1.41	23.28	0.15 ± 0.03	0.46	0.32 ± 0.06
TN-Flux (mg cm^{-2} y^{-1})	57.11 ± 8.08	173.06	1.26 ± 0.26	3.81	7.7 ± 1.49	23.33	0.15 ± 0.03	0.46	0.33 ± 0.06
IN-Flux (mg cm^{-2} y^{-1})	1.03 ± 0.36	103	0.02 ± 0.01	2.27	0.25 ± 0.09	25	0.005 ± 0.002	0.5	0.01 ± 0.001
BSi-Flux (mg cm^{-2} y^{-1})	578.91 ± 101.83	88.25	12.74 ± 3.26	1.94	91.52 ± 13.62	13.95	1.82 ± 0.27	0.28	6.56 ± 1.55
b[a]	11.43	–	2.10	–	4.47	–	−1.58	–	–
Δz (m)[b]	–	–	66.31	–	–	–	–	–	–
Range of Δz:Δdepth[c]	–	–	6.32–13.26	–	–	–	–	–	–

[a] b is the coefficient of flux attenuation, calculated by a power law equation: $F_z = F_{z_0}(z/z_0)^{-b}$, where F_z is the flux at depth z (sea bottom), normalized to flux at some reference depth, z_0 (sediment trap);
[b] Δz is the theoretical depth difference between sediment trap and sea bottom, calculated by an exponential equation: $F_z = F_{z_0}\exp(-\Delta z/z^*)$, where the remineralization length scale, z^*, defined as the depth interval over which the flux decreases by a factor of 1/e;
[c] Δz:Δdepth is the ratio of the theoretical depth difference to the actual depth with an range of 5 m to the total water column depth (10.5 m), representing the number of cycles required before final burial into the sediment.

resuspension correction, and the sedimented OC-flux at the surficial seabed (equivalent to F_z), were used to calculate *b*. The *b* values of stations TS1 and TS2 before correction were 11.43 and 4.47, respectively, while after correction they were 2.10 and −1.58, respectively (Table 2). Considering an open ocean composite *b* value of 0.86 derived from flux measurements in several North Pacific locations (Martin et al., 1987), and considering the regional variations of *b* values, ranging from 0.6 to 2.0 as demonstrated by deep-sea (> 2000 m) sediment trap studies (Francois et al., 2002), our values of *b* before calibration obviously exceed the normal range. After calibration, the value of TS1-*b* falls just above the higher limit of the range of previous studies, whereas the value of TS2-*b* is far below the range of reported values. This implies a faster attenuation of sinking particulate OC-flux through the lower part of the water column at station TS1 and a particulate OC-flux build-up at station TS2, which is obviously impracticable. Thus, the alternation of F_z by sedimented OC-flux would have propagated large uncertainties in the value of *b*. The attenuation of OC-flux with depth is a product of the remineralisation rate of organic material and the sinking speed of the OC-containing particles, both under the overall influences from community structure, mineral ballasting, temperature, and oxygen concentration (Turner, 2015). Nevertheless, a strong correlation of mesopelagic OC-flux attenuation with upper water column temperature was observed ($b = (0.062 \times T) + 0.303$, $r^2 = 0.82$, $p < 0.005$, Eq. (3)) (Marsay et al., 2015). Hence, the theoretical *b* values could be obtained by substituting the JZB temperatures (21.3 °C in July and 1 °C in November) into the *b*–T equation, which yielded $b = 1.624$ (TS1, July) and $b = 0.365$ (TS2, November). Then bring the theoretical *b* values backward into the Flux–Depth equation (Eq. (2)), the calculated flux reaching sea-floor should be 3.60 mg cm^{-2} y^{-1} for TS1 and 0.84 mg cm^{-2} y^{-1} for TS2, i.e. 48.2% attenuation for TS1 and 21.0% attenuation for TS2 would take place in the course of one settlement. Correspondingly, the middle value (2.97 ± 0.43 mg cm^{-2}

Table 3
Comparison of uncorrected and corrected settling flux of biogenic proxies at Jiaozhou Bay and analogues in adjacent sea-areas.

	Jiaozhou Bay	East China Sea (Autumn)	Yellow Sea (Autumn)	Yellow Sea (Summer)	Culture area of Sanggou Bay (Summer and Autumn)
Uncorrected Mass-Flux (g cm^{-2} y^{-1})	49.49 ± 5.09 (TS1) 8.68 ± 1.41 (TS2)	0.65–16.39 (18 m–83 m)	7.85 (35 m, E1) 6.04 (70 m, E2) 31.90 (40 m, E3)	2.92–11.46 (40 m–75 m)	55.17 of 10.15–97.36, (8 m) 15.45 of 0.25–33.75, (4 m)
Uncorrected OC-Flux (mg cm^{-2} y^{-1})	316.23 ± 35.06 (TS1) 53.41 ± 8.77 (TS2)	10.22–160.64 (18 m–83 m)	115.0 (35 m, E1) 81.03 (70 m, E2) 383.89 (40 m, E3)	44.34–148.96 (40 m–75 m)	730.4 of 145.6–1390, (8 m) 185 of 34–393.5, (4 m)
Uncorrected ON-Flux (mg cm^{-2} y^{-1})	56.08 ± 7.86 (TS1) 7.45 ± 1.41 (TS2)	1.06–11.46 (18 m–83 m)	6.3 (35 m, E1) 9.1 (70 m, E2) 25.5 (40 m, E3)	6.79–19.45 (40 m–75 m)	54.6 of 17–108.6, (8 m) 37.1 of 13.2–71.1, (4 m)
Uncorrected TN-Flux (mg cm^{-2} y^{-1})	57.11 ± 8.08 (TS1) 7.7 ± 1.49 (TS2)	–	–	17.3–57.3 (40 m–75 m)	17.3 of 0.66–59.6, (8 m) 9.8 of 0.55–22.2, (4 m)
Resuspension Ratio	97.8% (TS1) 98.01% (TS2)	66.5%–88.5%	89.53%–95.65%	90–96%	92.8% of 83.0–98.0%, (8 m) 80.4% of 44–94.9%, (4 m)
Corrected Mass-Flux (g cm^{-2} y^{-1})	1.09 ± 0.11 (TS1) 0.17 ± 0.03 (TS2)	–	0.17 (70 m, E2)	0.46 ± 0.13	1.97 of 0.9–2.8, (8 m) 1.5 of 0.14–2.36, (4 m)
Corrected OC-Flux (mg cm^{-2} y^{-1})	6.96 ± 1.12 (TS1) 1.06 ± 0.17 (TS2)	35.08 (55 m - upwelling zone) 4.49 (88 m – middle continental shelf)	7.008 (70 m, E2)	10.59 ± 1.46	25.9 of 7.7–41.6, (8 m) 21.2 of 6.9–31.4, (4 m)
Corrected ON-Flux (mg cm^{-2} y^{-1})	1.23 ± 0.25 (TS1) 0.15 ± 0.03 (TS2)	–	–	2.19 ± 0.37	0.66 of 0.04–2.04, (8 m) 0.8 of 0.11–1.6, (4 m)
Corrected TN-Flux (mg cm^{-2} y^{-1})	1.26 ± 0.26 (TS1) 0.15 ± 0.03 (TS2)	–	–	–	2.77 of 0.7–5.6, (8 m) 4.2 of 0.8–9.3, (4 m)
Reference	This study	Zhang et al. (2006c)	Zhang et al. (2005)	Zhang et al. (2004)	Yang et al. (2014)

The water depth and sampling station information were marked in parentheses, and 'mean value' of 'the variation range' were included in the last column.

y^{-1}) incorporated in SS (Table 2) might indicate: (i) perennial average level, (ii) early diagnosis reactions happened in bottom organic matter which triggered an actual greater TS1-*b* value (2.10), (iii) several re-suspension cycles and the alongside mineralization in water column could occur for TS1, which was further discussed below, and (iv) the limited bottom achieving contribution with a maximum of $0.84 \div 2.97 \times 100\% = 28.3\%$ for freshly biogenic particles produced in autumn/winter circumstances with low primary productivity like TS2.

Despite the simplicity of the above calculation, the power law equation is sensitive to the reference depth used (absolute depth or relative depth). A more advocated alternative approach proposed to describe OC-flux attenuation is the use of an exponential equation that relates the flux at any depth to the flux measured at a reference depth by the remineralisation length scale, z*, defined as the depth interval over which the flux decreases by a factor of 1/e (Buesseler and Boyd, 2009):

$$F_z = F_{z0} \exp(-\Delta z/z^*) \quad (4)$$

where Δz is the theoretical depth difference between sediment trap and sea floor. By establishing a good correlation between the calculated remineralisation length scale z* and the same temperature metric ($z^* = 483 - 19 \times T$, $r^2 = 0.74$, $p = 0.006$, Eq. (5)) (Marsay et al., 2015), it is easy to deduce that TS1 − z* = 78 m using the same temperature parameter. Considering the frequency of the resuspension process in JZB, we assumed that the difference between the corrected OC-flux and the sedimented analogue was entirely due to the process of water migration, i.e. neglecting the residence time of the SS and early diagenesis during this period. According to the Flux–Depth formula (Eq. (4)) proposed by Buesseler and Boyd (2009), the Δz between the sediment trap and the ocean bottom can be calculated, which is 66.63 m at TS1. After dividing the actual height difference (5 m) between the trap and the sea floor, it can be concluded that the freshly-formed biogenic particles will have to undergo [66.63/5] − 1 = 12 resuspension processes at similar heights before it can be buried in the sediment. In addition, considering the strongest re-suspension process that can carry particles to the surface layer, a minimum re-suspension process in summer (TS1) of [66.63/10.5] − 1 = 5 can be obtained by substituting the theoretical depth difference for the total water depth (10.5 m). This implies that a calculated 5–12 resuspension cycles would be required before final burial into the sediment record.

4.3. Evaluation of internal P sink-switching mechanism

As the lowest among the four IP forms, the loosely-absorbed and exchangeable P represented by P1 displayed a higher proportion for SS and CS5 (averaging 2.29% and 3.08%, respectively) than for TCP (typically < 2%) (Figs. 3 and 4), and was mainly attributed to the decomposition of organic matter (Yang et al., 2016). The phosphate ions liberated can adsorb to the surface of Fe oxides/hydroxides and clay minerals and are, therefore, the major carriers of P1, a mechanism reflected by the stronger relationship of P1 for silt ($r = 0.600$, $p = 0.000$) and sand ($r = -0.599$, $p = 0.000$) (Table A2). Thus, this indicates that elevated values of pore water phosphate (mainly as HPO_4^{2-}) is favorable for adsorption. Additionally, the grain size nature of the sedimentary matrix for which dissolved P interacts can influence the types of secondary phases formed under elevated pore-water phosphate conditions. Iron cycling is also a vital process for solid-phase P redistribution. The P2 fraction can be scavenged by ferric iron within aerobic regions of the sediment and/or water column and subsequently released when transported into reducing regions. Such an example of the redox state of bottom water and sediment being controlling parameters has been shown previously (Zhou et al., 2016). The sub-surface (4 cm) minimum of P2 concentration and percentage (Fig. 4) corresponded to an OP local minimum, which may reflect the reductive dissolution of ferric iron phases buried below the redox boundary. Hence it was reasonable to interpret the increasing P2 gradient above 4 cm as indicative of a barrier effect to diffusive loss from sediments and enhanced retention of P (Fig. 4). Nevertheless, both the comparable magnitude of P2 percent in TCP and SS/CS5, and the dampened variation of P2 along the CS5 depth profile, do not support a controlling role of iron cycling. A promising explanation for the absence of appreciable P2 abundance and variance in the coastal environment of JZB (Figs. 3 and 4), is that mineral Ca-bound P formed due to adsorption–precipitation switching across the estuarine salinity gradient as observed by Oxmann and Schwendenmann (2015). The gradual seaward decline in Fe−P, counterbalanced by the precipitation of Ca−P, has been discovered in numerous estuaries, including the Mississippi River estuary (Sutula et al., 2004), the Changjiang estuary (Meng et al., 2014), the Wanquan River estuary (Yang et al., 2016), and the Firth of Thames estuary (Oxmann and Schwendenmann, 2015). During increasing salinity/pH in the fresh-saline continuum, there is a shift of increasing competition between hydroxyl and phosphate ions for sorption sites and a decreasing surface electrostatic potential, particularly in concert with a declining Eh involving critical levels for the reduction of ferric iron compounds (e.g. (Gotoh and Patrick, 1974)). All of these facilitate desorption of iron oxides/hydroxides that are bound to P (Hartzell and Jordan, 2012; Hou et al., 2009). Therefore, the already affected P2 fraction would pose a negligible influence after reaching the offshore area, as supported by the matching TCP/CS5 reactive Fe_2O_3 concentrations (Fig. 2f) and the parallel molar P2:reactive Fe_2O_3 ratios (averaged at 4.594 for TCP and 4.588 for SS/CS5).

Notably, the near mirror-image relationship between OP and P3 in terms of both solid-phase concentration and proportion profile was illustrated in Fig. 4. This suggests that authigenic carbonate fluorapatite (CFA) is forming at the expense of OP, which has been liberated to the pore-water as a result of microbial remineralisation of organic matter. Such transfer of phosphorus from one reservoir to another (sink-switching) has been shown to be a ubiquitous phenomenon in the modern ocean, including "normal", terrigenous-dominated sediments in non-upwelling environments (Ruttenberg and Berner, 1993), which are characterized by relative high sediment accumulation rates and active winnowing and erosion as in JZB. Actually, the largest fraction of the SS/CS5-TP pool is in the authigenic CFA + biogenic apatite (fish bones, teeth and scales) + $CaCO_3$ reservoir. The negative coefficient of −0.56 for OP versus P3 for the whole dataset may be attributable to these possible non-CFA background phases. Nevertheless, the synchronized and near-quantitative transfer of dissolved P from remineralised organic matter to CFA implies that the loss of dissolved phosphate by diffusion out of the sediment prior to precipitation as CFA is minimal (Fig. 4).

This sink-switching mechanism indicates that sediments are retentive of P over the depth intervals sampled and is also applicable in the case of the TCP and SS comparison (Fig. 3). The P4, mainly derived from riverine input of terrestrial materials (Kang et al., 2017), displayed a consistent proportion in both TCP and SS/CS5, implying that the majority of sinking particles originated from resuspended particles with which terrestrial material incorporated/merged. Therefore, the 48.26% ~ 52.53% by which the OP concentration decreased from TCP to SS was primarily accounted for by the 30.19% ~ 37.49% increase in P3 concentration, one of two authigenic phases (the other is P2) (Fig. 3). Taken together with the negligible P1 proportion, and the 69.67% ~ 83.64% reduction in P2 for SS over TCP, this suggests that the bioavailable P (BAP, including P1, P2 and OP) represents the upper limit of P that can be released into the overlying water, given an appropriate physical and chemical environment (Meng et al., 2014), and would contribute to smaller levels in the SS. Thus, the resuspended P is likely to be significantly less bioavailable. Even though the dissolved P data was deficient, the low amount of sorbed P1 and declining P2 proportions in TCP/SS manifested in the form of limited/impoverished phosphate scavenging and deposition with solid particles in the water column following resuspension in the JZB.

5. Conclusion

From the present comparison study of the concentrations and stoichiometric ratios of different biogenic elements among surficial sediments (SS), core sediments (CS5), and settling trap-collected particles (TCPs), as well as a resuspension calibration, a flux attenuation analysis, and an internal P sink-switching assessment in the Jiaozhou Bay (JZB), the following conclusions can be drawn:

(1) The significantly higher concentrations of biogenic elements in the TCPs than in the surficial/core sediments can be attributed to two explanations: firstly, fine-grain-sized, highly selective resuspended particulate matter holds more organic constituents relative to non-suspended, coarse fractions; next, organic matter is degraded to a greater extent when migrating from the trap-deployed horizon to the sediment and during its residence at the sediment-water interface. The influence of decomposition, rather carbon source changes, was supported by multiple stoichiometric ratios (OC:ON and OC:OP) and IC concentrations in this study. The majority contribution of marine sourced OC was also manifested. The concentration of BSi in the TCP and sediments was about 10 mg g^{-1}, which can be affected by terrestrial clastic dilution, reverse weathering, and early diagenesis. The relationship between different stoichiometric ratios of bio-elements and the Redfield Ratio led us to deduce that the preservation efficiency of these bio-elements within organic matter is in the order of Si > C > N ≥ P; that is, P is the most easily lost bio-element and P-related ratios can effectively indicate the degradation processes of organic matter. Moreover, principal component analysis showed that the variation of biogenic elements in the overall dataset was predominantly controlled by three factors: the production and preservation of organic matter, the degradative processes, and the particle-size effect, which accounted for 55.5%, 14.0%, and 9.1% of the total variance, respectively.

(2) The sedimenting flux magnitudes of the organic indexes were in the order of OM-Flux > BSi- Flux > OC-Flux > ON-Flux > OP-Flux. After correcting for resuspension, the corrected sinking flux typically decreased by two orders of magnitude or more. Furthermore, the limited bottom achieving contribution with a maximum of 28.3% for freshly biogenic particles produced in autumn/winter circumstances with low primary productivity could be inferred. With respect to the frequency of resuspension processes in JZB, the corrected estimates suggest that the freshly-formed biogenic particles need to undergo 5–12 cycles of similar or higher intensity resuspension processes before they are finally buried in the sediments.

(3) There was a significant negative correlation ($r = -0.56$, $p = 0.00$) between organic and authigenic calcium-bound P. We also observed a near mirror-image relationship between the solid-phase concentration and proportion profiles of CS5. The implication is that P sink-switching from one reservoir to another has the potential to reduce dissolved phosphate diffusion and constrain bio-availability. Nevertheless, another authigenic P phase, iron-bound P, was subdued and moderated by adsorption–precipitation switching across the estuarine salinity gradient, leaving a narrow fluctuating gap for offshore redox cycling.

Acknowledgements

This research was funded by the National Basic Research Program (973) of China (No. 2015CB452902); the Aoshan Technology Innovation and Aoshan Talents Program Supported by Qingdao National Laboratory for Marine Science and Technology (No. 2016ASKJ02-4); the National Key Research and Development Plan Sino-Australian Centre for Healthy Coasts (No. 2016YFE0101500), the Youth Innovation Promotion Association, Chinese Academy of Sciences (No. 2016191) and the Joint Fund between Natural Science Foundation of China and Shandong Province (No. U1606404).

Appendix A. Supplementary data

Supplementary data to this article can be found online at https://doi.org/10.1016/j.jmarsys.2019.04.001.

References

Aspila, K.I., Agemian, H., Chau, A.S.Y., 1976. A semi-automated method for the determination of inorganic, organic and total phosphate in sediments. Analyst 101, 187–197.
Boyd, P.W., Trull, T.W., 2007. Understanding the export of biogenic particles in oceanic waters: is there consensus? Prog. Oceanogr. 72, 276–312.
Brea, S., Álvarez-Salgado, X.A., Álvarez, M., Pérez, F.F., Mémery, L., Mercier, H., Messias, M.J., 2004. Nutrient mineralization rates and ratios in the eastern South Atlantic. J. Geophys. Res. Oceans 109, C05030.
Brzezinski, M.A., 1985. THE Si:C:N ratio of marine diatoms: interspecific variability and the effect of some environmental variables. J. Phycol. 21, 347–357.
Buesseler, K.O., Boyd, P.W., 2009. Shedding light on processes that control particle export and flux attenuation in the twilight zone of the open ocean. Limnol. Oceanogr. 54, 1210–1232.
DeMaster, D.J., 1981. The supply and accumulation of silica in the marine environment. Geochim. Cosmochim. Acta 45, 1715–1732.
Demaster, D.J., 1991. Measuring Biogenic Silica in Marine Sediments and Suspended Matter, Marine Particles: Analysis and Characterization. American Geophysical Union, pp. 363–367.
DeMaster, D.J., 2002. The accumulation and cycling of biogenic silica in the Southern Ocean: revisiting the marine silica budget. Deep-Sea Res. II Top. Stud. Oceanogr. 49, 3155–3167.
Emerson, S., Bender, M., 1981. Carbon fluxes at the sedimentwater interface of the deep sea: calcium carbonate preservation. J. Mar. Res. 39, 139–162.
Folk, R.L., Ward, W.C., 1957. Brazos River bar [Texas]; a study in the significance of grain size parameters. J. Sediment. Petrol. 27, 3–26.
Francois, R., Honjo, S., Krishfield, R., Manganini, S., 2002. Factors controlling the flux of organic carbon to the bathypelagic zone of the ocean. Glob. Biogeochem. Cycles 16, 1087.
Frings, P.J., Clymans, W., Jeppesen, E., Lauridsen, T.L., Struyf, E., Conley, D.J., 2014. Lack of steady-state in the global biogeochemical Si cycle: emerging evidence from lake Si sequestration. Biogeochemistry 117, 255–277.
Galloway, J.M., Wigston, A., Patterson, R.T., Swindles, G.T., Reinhardt, E., Roe, H.M., 2013. Climate change and decadal to centennial-scale periodicities recorded in a late Holocene NE Pacific marine record: examining the role of solar forcing. Palaeogeogr. Palaeoclimatol. Palaeoecol. 386, 669–689.
Gardner, W.D., Southard, J.B., Hollister, C.D., 1985. Sedimentation, resuspension and chemistry of particles in the northwest Atlantic. Mar. Geol. 65, 199–242.
Gotoh, S., Patrick, W.H., 1974. Transformation of iron in a waterlogged soil as influenced by redox potential and pH 1. Soil Sci. Soc. Am. J. 38, 66–71.
Hartzell, J.L., Jordan, T.E., 2012. Shifts in the relative availability of phosphorus and nitrogen along estuarine salinity gradients. Biogeochemistry 107, 489–500.
Hedges, J.I., Mann, D.C., 1979. The characterization of plant tissues by their lignin oxidation products. Geochim. Cosmochim. Acta 43, 1803–1807.
Holligan, P.M., Harris, R.P., Newell, R.C., Harbour, D.S., Head, R.N., Linley, E., Lucas, M.I., Tranter, P., Weekley, C.M., 1984. Vertical distribution and partitioning of organic carbon in mixed, frontal and stratified waters of the English cannel. Orv. Hetil. 14, 111–127.
Honjo, S., Manganini, S.J., Krishfield, R.A., Francois, R., 2008. Particulate organic carbon fluxes to the ocean interior and factors controlling the biological pump: a synthesis of global sediment trap programs since 1983. Prog. Oceanogr. 76, 217–285.
Hou, L., Liu, M., Yang, Y., Ou, D., Lin, X., Chen, H., Xu, S., 2009. Phosphorus speciation and availability in intertidal sediments of the Yangtze Estuary, China. Appl. Geochem. 24, 120–128.
Huerta-Diaz, M.A., Tovar-Sánchez, A., Filippelli, G., Latimer, J., Sañudo-Wilhelmy, S.A., 2005. A combined CDB-MAGIC method for the determination of phosphorus associated with sedimentary iron oxyhydroxides. Appl. Geochem. 20, 2108–2115.
Hung, C., Tseng, C., Gong, G., Chen, K., Chen, M., Hsu, S., 2013. Fluxes of particulate organic carbon in the East China Sea in summer. Biogeosciences 10, 6469–6484.
Hung, C., Chen, Y., Hsu, S., Wang, K., Chen, J., Burdige, D.J., 2016. Using rare earth elements to constrain particulate organic carbon flux in the East China Sea. Sci. Rep. 6, 33880.
Hwang, J., Manganini, S.J., Park, J., Montlucon, D.B., Toole, J.M., Eglinton, T.I., 2017. Biological and physical controls on the flux and characteristics of sinking particles on the Northwest Atlantic margin. J. Geophys. Res. Oceans 122, 4539–4553.
Ingall, E.D., Cappellen, P.V., 1990. Relation between sedimentation rate and burial of organic phosphorus and organic carbon in marine sediments. Geochim. Cosmochim. Acta 54, 373–386.
Kaiser, H.F., 1958. The varimax criterion for analytic rotation in factor analysis. Psychometrika 23, 187–200.
Kalnejais, L.H., Martin, W.R., Bothner, M.H., 2010. The release of dissolved nutrients and metals from coastal sediments due to resuspension. Mar. Chem. 121, 224–235.
Kang, X., Song, J., Yuan, H., Shi, X., Yang, W., Li, X., Li, N., Duan, L., 2017. Phosphorus speciation and its bioavailability in sediments of the Jiaozhou Bay. Estuar. Coast.

Shelf Sci. 188, 127–136.
Lamb, A.L., Wilson, G.P., Leng, M.J., 2006. A review of coastal palaeoclimate and relative sea-level reconstructions using $\delta^{13}C$ and C/N ratios in organic material. Earth-Sci. Rev. 75, 29–57.
Li, L., Liu, S., Zhou, Z., Chao, L., 2010. Distribution of biogenic elements in the southern and central Bohai Sea sediments. Mar. Sci. 34, 59–68.
Liang, X., Song, J., Duan, L., Yuan, H., Li, X., Li, N., Qu, B., Wang, Q., Xing, J., 2018. Source identification and risk assessment based on fractionation of heavy metals in surface sediments of Jiaozhou Bay, China. Mar. Pollut. Bull. 128, 548–556.
Likens, G.E., Herbertbormann, F., Johnson, N.M., 1981. Interactions between Major Biogeochemical Cycle in Terrestrial Ecosystems. Some Perspectives of the Major Biogeochemical Cycles. pp. 93–112.
Lin, W., Chen, L., Zeng, S., Li, T., Wang, Y., Yu, K., 2016. Residual β activity of particulate ^{234}Th as a novel proxy for tracking sediment resuspension in the ocean. Sci. Rep. 6, 27069.
Liu, S., Ye, X., Zhang, J., Zhao, Y., 2002. Problems with biogenic silica measurement in marginal seas. Mar. Geol. 192, 383–392.
Liu, S., Zhang, J., Chen, H., Zhang, G., 2005. Factors influencing nutrient dynamics in the eutrophic Jiaozhou Bay, North China. Prog. Oceanogr. 66, 66–85.
Liu, S., Zhu, B., Zhang, J., Wu, Y., Liu, G., Deng, B., Zhao, M., Liu, G., Du, J., Ren, J., Zhang, G., 2010. Environmental change in Jiaozhou Bay recorded by nutrient components in sediments. Mar. Pollut. Bull. 60, 1591–1599.
Liu, J., Ye, S., Allen Laws, E., Xue, C., Yuan, H., Ding, X., Zhao, G., Yang, S., He, L., Wang, J., Pei, S., Wang, Y., Lu, Q., 2016. Sedimentary environment evolution and biogenic silica records over 33,000 years in the Liaohe delta, China. Limnol. Oceanogr. 62, 474–489.
Liu, J., Ye, S., Yuan, H., Ding, X., Zhao, G., Yang, S., He, L., Wang, J., Pei, S., Huang, X., 2018. Metal pollution across the upper delta plain wetlands and its adjacent shallow sea wetland, northeast of China: implications for the filtration functions of wetlands. Environ. Sci. Pollut. Res. 25, 5934–5949.
Loucaides, S., Michalopoulos, P., Presti, M., Koning, E., Behrends, T., Van Cappellen, P., 2010. Seawater-mediated interactions between diatomaceous silica and terrigenous sediments: results from long-term incubation experiments. Chem. Geol. 270, 68–79.
Marsay, C.M., Sanders, R.J., Henson, S.A., Pabortsava, K., Achterberg, E.P., Lampitt, R.S., 2015. Attenuation of sinking particulate organic carbon flux through the mesopelagic ocean. Proc. Natl. Acad. Sci. 112, 1089–1094.
Martin, J.H., Knauer, G.A., Karl, D.M., Broenkow, W.W., 1987. VERTEX: carbon cycling in the northeast Pacific. Deep-Sea Res. I Oceanogr. Res. Pap. 34, 267–285.
Matisoff, G., Carson, M.L., 2014. Sediment resuspension in the Lake Erie nearshore. J. Great Lakes Res. 40, 532–540.
Mayer, L.M., 1994. Surface area control of organic carbon accumulation in continental shelf sediments. Geochim. Cosmochim. Acta 58, 1271–1284.
Meinhard, S., Hans-Peter, G., Bernd, S., Helle, P., 2002. Microbial ecology of organic aggregates in aquatic ecosystems. Aquat. Microb. Ecol. 28, 175–211.
Meng, J., Yao, P., Yu, Z., Bianchi, T.S., Zhao, B., Pan, H., Li, D., 2014. Speciation, bioavailability and preservation of phosphorus in surface sediments of the Changjiang Estuary and adjacent East China Sea inner shelf. Estuar. Coast. Shelf Sci. 144, 27–38.
Meyers, P.A., Leenheer, M.J., Eadie, B.J., Maule, S.J., 1984. Organic geochemistry of suspended and settling particulate matter in Lake-Michigan. Geochim. Cosmochim. Acta 48, 443–452.
Michalopoulos, P., Aller, R.C., 1995. Rapid clay mineral formation in Amazon Delta sediments: reverse weathering and oceanic elemental cycles. Science 270, 614–617.
Moriarty, J.M., Harris, C.K., Fennel, K., Friedrichs, M.A.M., Xu, K., Rabouille, C., 2017. The roles of resuspension, diffusion and biogeochemical processes on oxygen dynamics offshore of the Rhone River, France: a numerical modeling study. Biogeosciences 14, 1919–1946.
Mortlock, R.A., Froelich, P.N., 1989. A simple method for the rapid determination of biogenic opal in pelagic marine sediments. Deep-Sea Res. I Oceanogr. Res. Pap. 36, 1415–1426.
Ni, J., Lin, P., Zhen, Y., Yao, X., Guo, L., 2015. Distribution, source and chemical speciation of phosphorus in surface sediments of the central Pacific Ocean. Deep-Sea Res. I Oceanogr. Res. Pap. 105, 74–82.
Oxmann, J.F., Schwendenmann, L., 2015. Authigenic apatite and octacalcium phosphate formation due to adsorption-precipitation switching across estuarine salinity gradients. Biogeosciences 12, 723–738.
Painter, S.C., Hartman, S.E., Kivimäe, C., Salt, L.A., Clargo, N.M., Daniels, C.J., Bozec, Y., Daniels, L., Allen, S., Hemsley, V.S., Moschonas, G., Davidson, K., 2017. The elemental stoichiometry (C, Si, N, P) of the Hebrides Shelf and its role in carbon export. Prog. Oceanogr. 159, 154–177.
Pichevin, L.E., Ganeshram, R.S., Geibert, W., Thunell, R., Hinton, R., 2014. Silica burial enhanced by iron limitation in oceanic upwelling margins. Nat. Geosci. 7, 541–546.
Poulton, S.W., Canfield, D.E., 2005. Development of a sequential extraction procedure for iron: implications for iron partitioning in continentally derived particulates. Chem. Geol. 214, 209–221.
Prahl, F.G., Bennett, J.T., Carpenter, R., 1980. The early diagenesis of aliphatic hydrocarbons and organic matter in sedimentary particulates from Dabob Bay, Washington. Geochim. Cosmochim. Acta 44, 1967–1976.
Pusceddu, A., Grémare, A., Escoubeyrou, K., Amouroux, J.M., Fiordelmondo, C., Danovaro, R., 2005. Impact of natural (storm) and anthropogenic (trawling) sediment resuspension on particulate organic matter in coastal environments. Cont. Shelf Res. 25, 2506–2520.
Redfield, A.C., Ketchum, B.H., Richards, F.A., 1963. The Influence of Organisms on the Composition of Sea-water. The Sea, New York, pp. 26–77.
Reimers, C.E., Kastner, M., Garrison, R.E., 1989. The role of bacterial mats in phosphate mineralization with particular reference to the Monterey Formation. In: Burnett, W.C., Riggs, S.R. (Eds.), Genesis of Neogene to Modern Phosphorites. Cambridge University Press, United States.
Rutgers van der Loeff, M.M., Boudreau, B.P., 1997. The effect of resuspension on chemical exchanges at the sediment-water interface in the deep sea — a modelling and natural radiotracer approach. J. Mar. Syst. 11, 305–342.
Ruttenberg, K.C., 1992. Development of a sequential extraction method for different forms of phosphorus in marine sediments. Limnol. Oceanogr. 37, 1460–1482.
Ruttenberg, K.C., Berner, R.A., 1993. Authigenic apatite formation and burial in sediments from non-upwelling, continental margin environments. Geochim. Cosmochim. Acta 57, 991–1007.
Song, J., Li, X., 2018. Ecological functions and biogenic element cycling roles of marine sediment/particles. Haiyang Xuebao 40, 1–13.
Song, J., Duan, L., Yuan, H., 2016. The Evolution of the Chemical Environment in the Jiaozhou Bay. Science Press, Beijing.
Sutula, M., Bianchi, T.S., McKee, B.A., 2004. Effect of seasonal sediment storage in the lower Mississippi River on the flux of reactive particulate phosphorus to the Gulf of Mexico. Limnol. Oceanogr. 49, 2223–2235.
Turner, J.T., 2015. Zooplankton fecal pellets, marine snow, phytodetritus and the ocean's biological pump. Prog. Oceanogr. 130, 205–248.
Xing, J., Song, J., Yuan, H., Li, X., Li, N., Duan, L., Kang, X., Wang, Q., 2017. Fluxes, seasonal patterns and sources of various nutrient species (nitrogen, phosphorus and silicon) in atmospheric wet deposition and their ecological effects on Jiaozhou Bay, North China. Sci. Total Environ. 576, 617–627.
Xing, J., Song, J., Yuan, H., Wang, Q., Li, X., Li, N., Duan, L., Qu, B., 2018. Water-soluble nitrogen and phosphorus in aerosols and dry deposition in Jiaozhou Bay, North China: deposition velocities, origins and biogeochemical implications. Atmos. Res. 207, 90–99.
Xu, Q., Yang, H., 2007. Food sources of three bivalves living in two habitats of Jiaozhou Bay (Qingdao, China): indicated by lipid biomarkers and stable isotope analysis. J. Shellfish Res. 26, 561–567.
Yang, L., Wu, Y., Zhang, J., Liu, S., Deng, B., 2011. Burial of terrestrial and marine organic carbon in Jiaozhou Bay: different responses to urbanization. Reg. Environ. Chang. 11, 707–714.
Yang, Q., Yang, S., Song, X., Sun, Y., 2014. Vertical flux and resuspension of settling particulate matter of Sanggou Bay in summer and autumn. Acta Oceanol. Sin. 36, 85–90.
Yang, B., Liu, S., Wu, Y., Zhang, J., 2016. Phosphorus speciation and availability in sediments off the eastern coast of Hainan Island, South China Sea. Cont. Shelf Res. 118, 111–127.
Ye, X., Liu, S., Zhang, J., 2002. Ditermination of biogenic opal in sediment of the Huanghai and Bohai Sea and questions in the method. Acta Oceanol. Sin. 24, 129–134.
Ye, S., Laws, E.A., Gambrell, R., 2013. Trace element remobilization following the resuspension of sediments under controlled redox conditions: City Park Lake, Baton Rouge, LA. Appl. Geochem. 28, 91–99.
Yu, Y., Song, J., Li, X., Duan, L., 2012a. Geochemical records of decadal variations in terrestrial input and recent anthropogenic eutrophication in the Changjiang Estuary and its adjacent waters. Appl. Geochem. 27, 1556–1566.
Yu, Y., Song, J., Li, X., Yuan, H., Li, N., 2012b. Distribution, sources and budgets of particulate phosphorus and nitrogen in the East China Sea. Cont. Shelf Res. 43, 142–155.
Yu, Y., Song, J., Li, X., Yuan, H., Li, N., Duan, L., 2013. Environmental significance of biogenic elements in surface sediments of the Changjiang Estuary and its adjacent areas. J. Environ. Sci. 25, 2185–2195.
Yurkovskis, A., 2005. Seasonal benthic nepheloid layer in the Gulf of Riga, Baltic Sea: sources, structure and geochemical interactions. Cont. Shelf Res. 25, 2182–2195.
Zhang, Y., Zhang, F., Guo, X., Zhang, M., 2004. Vertical flux of the settling particulate matter in the water column of the Yellow Sea in summer. Oceanologia et Limnologia Sinica 35, 230–238.
Zhang, Y., Zhang, F., Guo, X., Zhang, M., 2005. Autumn vertical flux of settling particulate matter at three typical stations in the Yellow Sea. Geochimica 34, 123–128.
Zhang, N., Song, J., He, Z., 2006a. Biogeochemical mechanism of particulate organic carbon (POC) variations in seawaters. Acta Ecol. Sin. 26, 2328–2339.
Zhang, Y., Zhang, F., Guo, X., Zhang, M., 2006b. Autumn flux of particle settling observed at three represenative stations in east China sea. Oceanologia et Limnologia Sinica 37, 28–34.
Zhang, Y., Zhang, F., Guo, X., Zhang, M., 2006c. Autumn flux of particle settling observed at three representative stations in East China Sea. Oceanologia et Limnologia Sinica 37, 28–34.
Zhou, F., Gao, X., Yuan, H., Song, J., Chen, C.-T.A., Lui, H.-K., Zhang, Y., 2016. Geochemical forms and seasonal variations of phosphorus in surface sediments of the East China Sea shelf. J. Mar. Syst. 159, 41–54.